Anisotropically Hybridized Porous Crystalline Li-S Battery Separators

Yuluan Zhang, Can Guo, Jie Zhou, Xiaoman Yao, Jie Li, Huifen Zhuang, Yuting Chen, Yifa Chen,* Shun-Li Li, and Ya-Qian Lan*

Anisotropically hybridized porous crystalline Li-S battery separators based on porous crystalline materials that can meet the multiple functionalities of both anodic and cathodic sides are much desired for Li-S battery yet still challenging in directional design. Here, an anisotropically hybridized separator (CPM) based on an ionic liquid-modified porphyrin-based covalent-organic framework (COF-366-OH-IL) and catalytically active metal-organic framework ($Ni_3(HITP)_2$) that can integrate the lithium-polysulfides (LiPSs) adsorption/catalytic conversion and ion-conduction sites together to directionally meet the requirements of electrodes is reported. Remarkably, the-obtained separator exhibits an exceptional high Li^+ transference-number ($t_{Li+} = 0.8$), ultralow polarization-voltage (<30 mV), high initial specific-capacity (921.38 mAh g^{-1} at 1 C), and stable cycling-performance, much superior to polypropylene and monolayer-modified separators. Moreover, theoretical calculations confirm the anisotropic effect of CPM on the anodic side (e.g., Li^+ transfer, LiPSs adsorption, and anode-protection) and cathodic side (e.g., LiPSs adsorption/catalysis). This work might provide a new perspective for separator exploration.

1. Introduction

As current trends in energy utilization and new energy supply evolve, battery technology has become a critical issue for sustainable energy conversion and storage. Currently, Li-ion battery has gradually been unable to meet the requirements of practical applications due to the limited energy density and poor safety.[1,2] At the same time, lithium-sulfur (Li-S) battery with high theoretical specific capacity (1675 mAh g^{-1})/energy density (2600 Wh kg^{-1}), and abundant stock of cathode materials with low cost are considered the most promising candidates for next-generation battery systems.[3–5] So far, the research on Li-S

battery is still limited due to its inherent disadvantages (sluggish reaction kinetics, the shuttle effect of polysulfides (LiPSs), the generation of lithium dendrites, etc.), which needs much effort to be made for advanced techniques.[6–9] As an important part in Li-S battery, separators play a profound role in solving the above shortcomings. And also an ideal separator needs to satisfy the following properties/features: 1) good abilities in adsorption/catalysis of LiPSs to suppress the shuttle effect;[10] 2) high porosity, excellent electrolyte wettability and long-lasting electrolyte retention for efficient Li^+ transfer, and thus high electrochemical stability to resist electrolyte corrosion is also necessary;[11] 3) high mechanical/thermal stability to sustain the long operation and tolerate dendrite formation.[12,13] Currently, commercial separators are mainly olefin separators such as polypropylene (PP) or polyethylene (PE), etc. However, their disadvantages like low wettability to the electrolyte, poor Li^+/electrolyte transport and strong shuttle effect limit the performance of Li-S battery. Therefore, separator engineering strategy like the modification of commercial PP is regarded as one of the most effective approaches to address the challenging problems of Li-S battery separators.[14–16]

In reality, the requirements for the separator are diversified due to the different environments on both electrode sides. Functional layers facing sulfur (S) cathode should be considered firstly for LiPSs adsorption/catalysis, as well as serving as electron conductive interlayer for smooth transfer of electrons from the electrode to the interlayer region.[17–19] Meanwhile, an anodic interlayer will be provided with electron insulation property while maintaining fast Li^+ transport and anode protection ability to inhibit dendrite growth.[20,21] Therefore, it is necessary to modify PP by anisotropic hybridization of materials with different properties. Combining the functions required for the modified layers on both sides of PP, the basic design principle of anisotropically hybridized separators is that the anodic side layer should be insulating and porous with high Li^+ mobility and meanwhile, the cathodic layer is preferably conductive with excellent LiPSs adsorption/catalysis ability. As far as know, such kind of PP-modified separator for Li-S battery has been rarely reported and remains a challenge to be explored.

Y. Zhang, C. Guo, J. Zhou, X. Yao, J. Li, H. Zhuang, Y. Chen, Y. Chen,
S.-L. Li, Y.-Q. Lan
School of Chemistry
National and Local Joint Engineering Research Center of MPTES in High
Energy and Safety LIBs
Engineering Research Center of MTEES (Ministry of Education)
and Key Lab. of ETESPG(GHEI)
South China Normal University
Guangzhou 510006, P. R. China
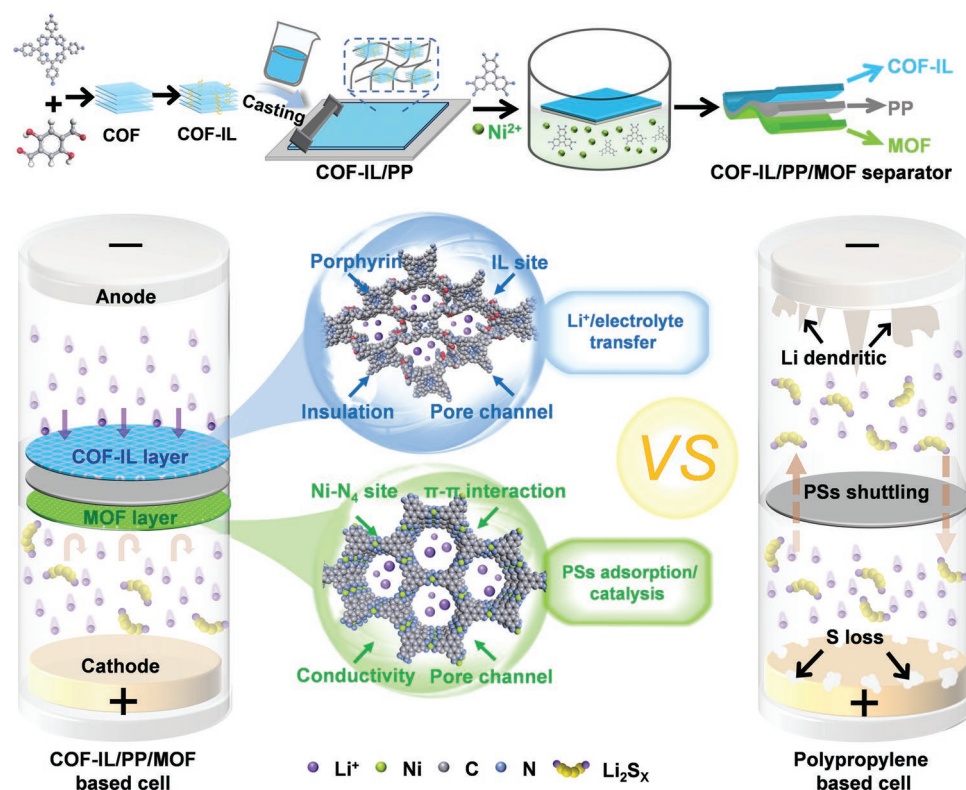E-mail: chyf927821@163.com; yqlan@m.scnu.edu.cn

ADVANCED
SCIENCE NEWS
www.advancedsciencenews.com

NANO · MICRO
small
www.small-journal.com

Porous crystalline materials including metal-organic frameworks (MOFs) and covalent organic frameworks (COFs) have been applied in many fields like energy storage,[22,23] biomedicine,[24,25] photo-/electro-catalysis,[26] gas adsorption/separation,[27] and sensing,[28,29] etc. Their tunable properties such as well-defined structure, high porosity, crystallinity, and modifiability confer many possibilities to be used as PP modifying materials for Li-S battery separators. Up to date, some pioneering works have applied MOFs (e.g., HKUST-1,[30] Ce-MOF,[31] or UIO-66-NH$_2$,[32] etc.) or COFs (e.g., SCOF-1/2[33] or TAPP-ETTB COF,[34] etc.) based membranes as modification layers of PP. However, there are still some bottlenecks: 1) the works reported so far usually use only one kind of MOFs or COFs, which would hardly fulfill most of the requirements for Li-S battery separators; 2) the anisotropic function design that can satisfy the specific requirements of the diversified environment on each electrode side is generally neglected; and 3) the generally unbalanced one side modification of separator will lead to unavoidable cell polarization or increased impedance. In particular, it remains a daunting challenge to modify MOFs and COFs on both sides of PP to meet the multifunctional needs of the separators. Therefore, we prefer to construct an anisotropically hybridized separator based on ionic liquid modified porphyrin-based COF and catalytically active MOF to solve the problem of Li-S battery based on the following considerations: 1) conductive MOF with catalytic activity can catalyze the conversion of LiPSs while the conductive layer can achieve smooth electron transfer between layers and inhibit the escape of LiPSs;[35,36] 2) ionic liquid modified porphyrin-based COF (COF-IL) with insulation and organic substance nature can promote Li$^+$/electrolyte diffusion, provide extra LiPSs adsorption,[37,38] and homogenize the electric field of Li$^+$ deposition to inhibit dendrite formation; and 3) the combination of them as anisotropic, balanced and hybridized membrane might largely reduce the cell polarization or impedance. Taken together, such powerful anisotropic hybridized separators may fulfill the demand of high-efficiency Li-S battery, yet there are no relative reports to the best of our knowledge.

Here, we report an anisotropically hybridized Li-S battery separator (CPM) based on ionic liquid modified porphyrin-based COF (COF-366-OH-IL) and catalytically conductive MOF (Ni$_3$(HITP)$_2$) (**Scheme 1**). Combining the advantages of MOFs and COFs, the obtained three-layer anisotropically hybridized separator exhibits favorable electrolyte wettability, excellent robustness, and functional anisotropy of Li$^+$/electrolyte transfer, LiPSs adsorption/catalysis and reduction of cell polarization. Notably, the-obtained separator exhibits an exceptional high Li$^+$ transference-number ($t_{Li+} = 0.8$), ultralow polarization-voltage (<30 mV), high initial specific-capacity (921.38 mAh g^{-1} at 1 C) and stable cycling-performance, much superior to PP and monolayer modified separators. In addition, the anisotropic effects of CPM on the anodic side (e.g., Li$^+$ transfer, LiPSs adsorption, and anode-protection) and cathodic side (e.g., LiPSs adsorption/catalysis) have been intensively supported by density functional theory (DFT) calculations and sufficient characterization tests. The present work demonstrates the concept of rational construction of anisotropically hybridized separators may accelerate the applications of anisotropically hybridized porous crystalline membrane in energy storage.

Scheme 1. Schematic diagram of the anisotropically hybridized COF-IL/PP/MOF (CPM) and its advantages as Li-S battery separator.

**ADVANCED
SCIENCE NEWS**

www.advancedsciencenews.com

NANO · MICRO

small

www.small-journal.com

2. Results

2.1. Synthesis and Characterization of CPM

The synthesis processes of CPM separator are divided into two steps, including COF-IL layer and MOF layer modification steps on PP (Scheme 1). For the COF-IL layer, COF-366-OH was firstly prepared by a Schiff base reaction,[39] modified with ionic liquid[40] (i.e., 2-bromoethyltrimethylammonium bromide), and cast with poly(vinylidene fluoride-co-hexafluoropropylene) (PVDF-HFP) suspension onto commercial PP by a doctor blade. After drying, the obtained COF-IL/PP membrane was further placed on the surface of a mixed precursor solution of MOF (i.e., $Ni_3(HITP)_2$), and grown MOF based membrane with a certain time through an epitaxial growth strategy.[41,42] By adjusting the loading of COF-IL layer and the reaction time of MOF layer, we have obtained a series of CPM separators for further characterizations. Based on the evaluation of previously reported COF or MOF modified PP separators,[32,42] we firstly selected a typical COF-IL loading of 20 wt% and a MOF growth time of 3 h to study their basic properties. The photo images of it show high flexibility with a smooth and shiny surface for MOF membrane side and a relatively dark yet still smooth surface for COF-IL membrane side, respectively (**Figure 1**a). For the COF-IL
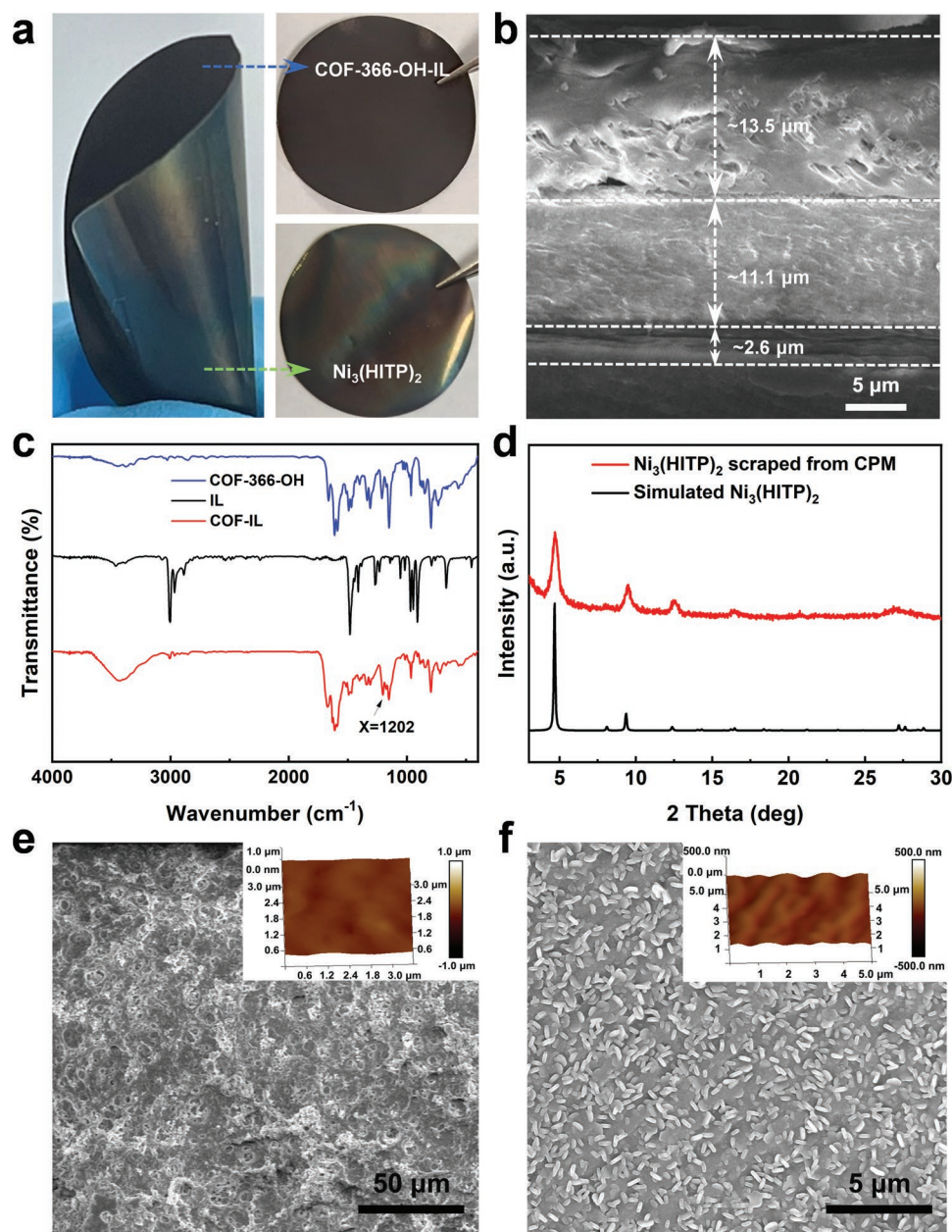

Figure 1. The characterizations of CPM. a) Photo images of CPM membrane. b) Cross section SEM image of CPM. c) FT-IR spectra of COF-366-OH, IL and COF-366-OH-IL. d) PXRD patterns of $Ni_3(HITP)_2$. e) SEM image of the COF-IL layer of CPM (insert is the 3D AFM image). f) SEM image of the $Ni_3(HITP)_2$ layer of CPM (insert is the 3D AFM image).

membrane side, the synthesis of COF-366-OH was confirmed by the powder X-ray diffraction (PXRD) tests[43] (Figure S1, Supporting Information). Fourier transform infrared spectroscopy (FT-IR) spectra of COF-IL displayed that the –OH characteristic peak at 1398 cm^{-1} disappeared coupled with the appearance of C–O–CH$_2$ characteristic peak at 1200 cm^{-1}, indicating the successful reaction of –OH and 2-bromoethyltrimethylammonium bromide (Figure 1c). For the MOF membrane side, the PXRD pattern of Ni$_3$(HITP)$_2$ powder scraped from the CPM membrane was consistent with its simulated one (Figure 1d), proving the successful formation of Ni$_3$(HITP)$_2$.[41]

To further study morphology, scanning electron microscopy (SEM) and transmission electron microscopy (TEM) tests had been carried out. The cross-sectional SEM image showed that the thicknesses of COF-IL layer and Ni$_3$(HITP)$_2$ layer were ≈13.5 and ≈2.6 μm, respectively, and they were tightly connected in cross-sections without any gaps or cracks (Figure 1b). For the COF-IL membrane side, SEM images showed that the spherical COF-IL nanoparticles with sizes of ≈380 nm were uniformly distributed in the membrane (Figure 1e and Figure S2, Supporting Information), further supported by the evenly distributed elemental mapping images of C, F, and N (Figure S3, Supporting Information). For the MOF membrane side, Ni$_3$(HITP)$_2$ nanoparticles in flake morphology with sizes of ≈600 nm were successfully grown on PP surface in the SEM tests (Figure 1f). The uniformity was further verified by the elemental mapping tests, in which Ni, N, and C were evenly distributed in the membrane (Figure S4, Supporting Information). The crystalline lattice in the high-resolution transmission electron microscopy (HRTEM) image showed its good crystallinity (Figure S5, Supporting Information). Moreover, atomic force microscopy (AFM) tests were further executed and show the flatter uniform 2D (Figures S6 and S7, Supporting Information) and 3D morphological image on both sides of CPM (Figure 1e,f).

After integrating COF-IL layer and Ni$_3$(HITP)$_2$ layer on both sides of PP in the CPM, the thus-produced hybrid membrane would inherit the advantages of them to exhibit high mechanical strength. As expected, the tensile stress tests showed that CPM had high stress of ≈12.55 MPa at ≈5.83% strain, which was almost doubly enhanced than that of pristine PP separator (stress, ≈6.0 MPa; strain, 11.7%) (**Figure 2**a). This result was also clearly demonstrated by the tensile test that a piece of CPM (width, 2.8 cm) could successfully tolerate a ≈5 kg barrel (Figure 2b). To investigate the LiPSs permeation capacity of separators, we conducted the shuttle tests.[44] As shown in Figure 2c, a dark red LiPSs solution was placed in a 1.5 mL glass vial sealed by a blue cap where the separator was fixed inside and then it was put upside-down in DOL/DME solution (v/v, 1:1) in a big bottle. The LiPSs permeation test showed that CPM could effectively inhibit the LiPSs shuttle for more than 10 h. This result was much better than that of PP, where its permeation occurred only after 5 min. The higher inhibition efficiency may be due to the synergistic effect of COF-IL layer and Ni$_3$(HITP)$_2$ layer in CPM. Moreover, contact angle tests have been conducted to evaluate the electrolyte wettability of different separators. The introduced CPM separator can result in decreased contact angle of both sides for CPM (i.e., COF-IL layer, 14.7° and Ni$_3$(HITP)$_2$ layer, 18.1°) when compared with

that of PP (31.0°), displaying excellent wettability of the CPM separator to the electrolyte (Figure S8, Supporting Information).

2.2. Battery Performance

As mentioned above, the combination of porosity, high mechanical strength, and LiPSs inhibition in CPM makes it to be a potential separator candidate for Li-S battery. To investigate the cell performance, conventional electrochemical tests such as constant current charge/discharge, cyclic voltammetry (CV), and electrochemical impedance spectroscopy (EIS) had been tested with CPM as the separator, sulfur-carbon complex (CNT)/S (S content, 70 wt%) as the cathode material and lithium metal foil as the anode.[45] For comparison, the performance of pure PP based Li-S cell was also tested. CV experiments reveal the conversion of LiPSs within the battery (Figure S9, Supporting Information). The CV curves of CPM based Li-S cells showed two reduction peaks centered at 2.3 and 2.0 V, indicating the reduction of sulfur to soluble LiPSs (Li$_2$S$_n$, 4 < n < 8) and further reduction to solid lithium sulfide (Li$_2$S$_2$/Li$_2$S), respectively (**Figure 3**a).[46] In addition, the rate performance of the cell was evaluated by constant current charge/discharge from 0.1 to 2 C within a potential window of 1.7–2.6 V. It can be seen that the initial capacity of the CPM based Li-S cell is 1088.7 mAh g^{-1} at 0.1 C, which is 166 mAh g^{-1} larger than that of PP based Li-S cell. In terms of capacity, the CPM based Li-S cell provided 665.9, 569.3, 507.5, 476.3, and 444.6 mAh g^{-1} at the rates of 0.2, 0.3, 0.5, 1, and 2 C, respectively. The performance was superior to that of PP based Li-S cell, which declined rapidly with increasing current density (Figure 3c). The additional capacity may be due to the effective inhibition of LiPSs shuttle, resulting in the high utilization of active materials. Finally, the capacity returns to 530.2 mAh g^{-1} at 0.2 C, indicating a good rate performance of the cell. Cycling stability is crucial for the long-term application of Li-S battery. The cycling tests of different separators were investigated by constant current charge/discharge tests at 1 C. The initial capacity was 921.4 mAh g^{-1} and it could be cycled for more than 300 cycles, which was much superior to PP based Li-S cell (Figure 3e). In addition, we also performed the EIS tests of CPM and PP based Li-S cells to evaluate their resistance. The semicircle in the high-frequency region of Nyquist plots was attributed to the charge transfer resistance (R_{ct}) and the straight line in the low-frequency region corresponded to a mass transfer process. It could be seen that the R_{ct} value of CPM based Li-S cell (23.8 Ω) was lower than PP based Li-S cell (25.3 Ω), indicating its faster electron transfer (Figure S10, Supporting Information). To further set out to explore the superiority of the anisotropically hybridized porous crystalline architecture of CPM, PP modified with only COF-IL layer (i.e., COF-IL/PP) or MOF layer (i.e., Ni$_3$(HITP)$_2$/PP) have been prepared as comparison samples. The COF-IL/PP based Li-S cell reserved 555.0 mAh g^{-1} after 100 cycles at 0.2 C, which is slightly higher than Ni$_3$(HITP)$_2$/PP based Li-S cell (451.8 mAh g^{-1} after 100 cycles) yet still much lower than CPM based Li-S cell (Figure 3d). The EIS tests present similar Nyquist plots and showed that the R_{ct} of Ni$_3$(HITP)$_2$/PP (41.9 Ω) was lower than that of COF-IL/PP (53.6 Ω), which implied a faster electron transfer efficiency between electrode
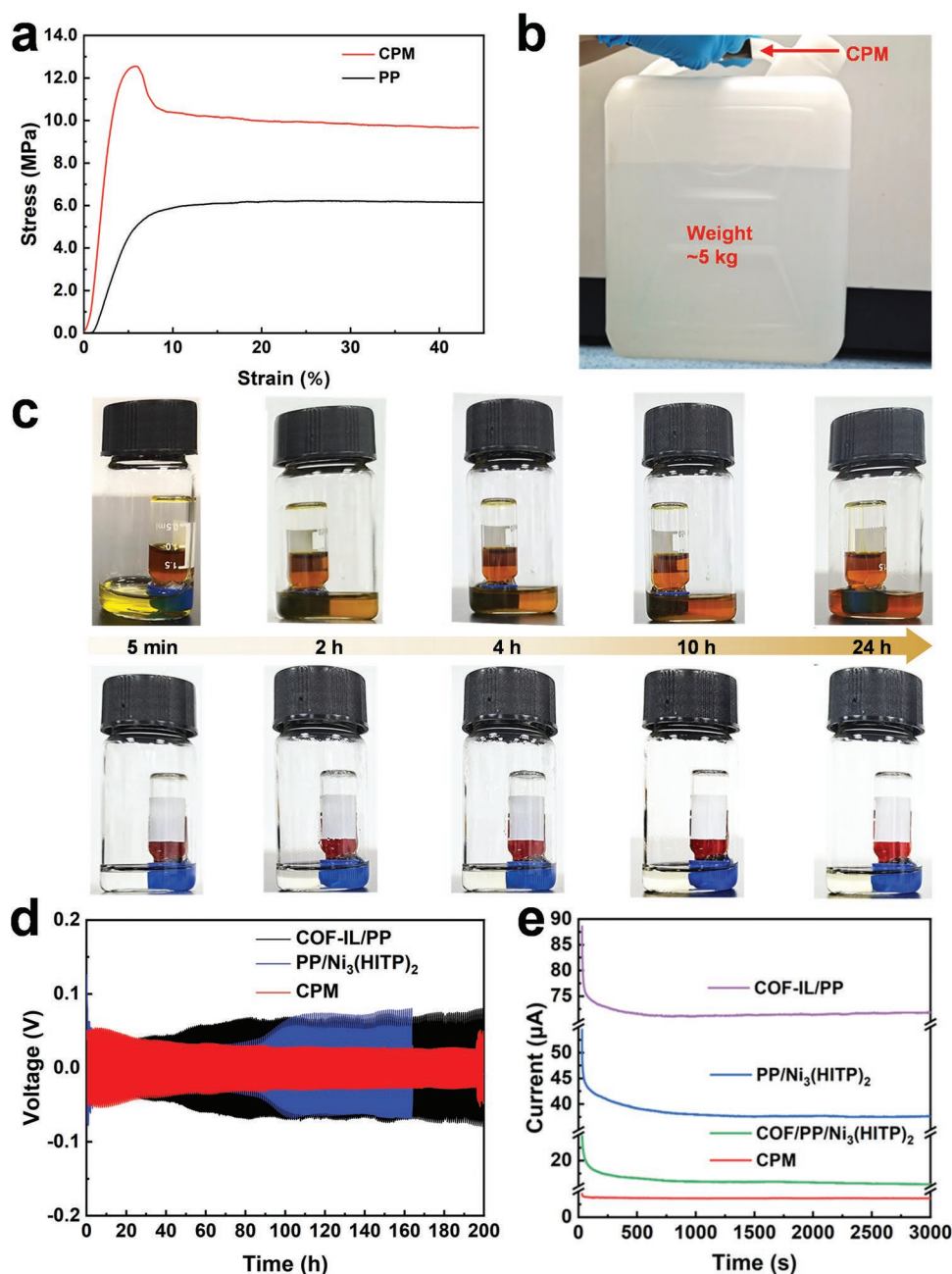
Figure 2. The characterizations and symmetric cell tests of CPM separator. a) Stress–strain curve of CPM membrane and PP. b) Photo image of the tensile stress experiment for CPM (width, ≈2.8 cm) with a ≈5 kg barrel holding downside. c) LiPSs permeation tests of PP (above) and CPM (below). d) Galvanostatic cycling of symmetric cells with different separators. e) Chronoamperometry profiles for different separators.

and electrolyte that might be attributed to the higher electron conducting nature of $Ni_3(HITP)_2$ layer (Figure S10, Supporting Information). However, the R_{ct} of $Ni_3(HITP)_2/PP$ was still much larger than the CPM (23.8 Ω), suggesting that the anisotropic hybridization may reduce the polarization and play a significant role in reducing the impedance. Combined with the slope in the low frequency region, it can be seen that the CPM based cell is more favorable for the diffusion of Li^+.

To investigate the ability of anisotropic hybrid separators to migrate in Li and their superiority over the monolayer modified separators, time-ampere (CA) tests and cycling performance

of Li//Li symmetric cell were performed.[14,47] We tested the constant current cycling performance of the symmetric Li//Li symmetric cell charged/discharged at 0.3 mA cm^{-2} to further investigate the Li^+ transport-induced polarization phenomenon. After 190 h, the polarization voltage of the specially designed CPM separator could be stably maintained at 25 mV, and the performance was better than that of the single-layer modified separator, which was attributed to the ability of CPM might effectively suppress the battery polarization and promote the rapid transfer of Li^+/electrolytes (Figure 2d). The charge/discharge profiles in cycle tests with different separators
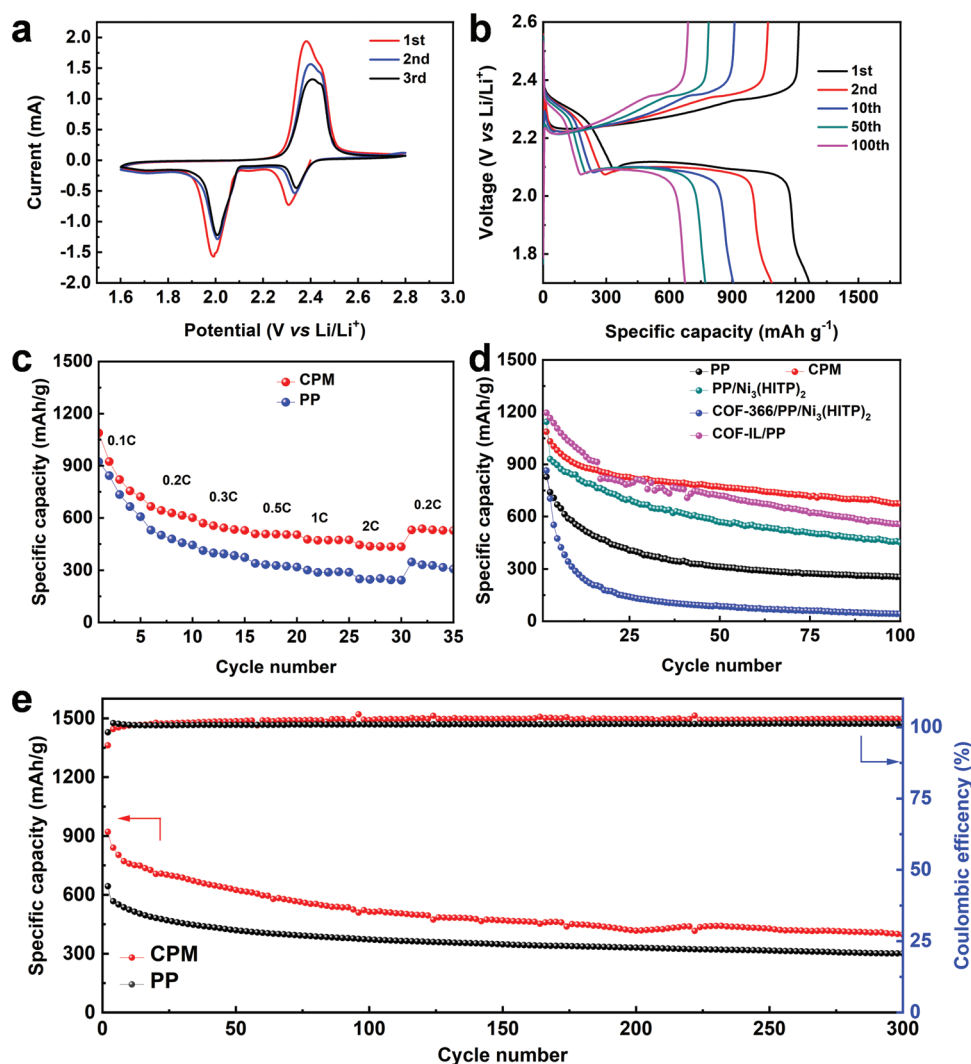
Figure 3. The cell performances of CPM based Li-S cells. a) CV curves tested at a scan rate of 0.1 mV s^{-1}. b) Charge/discharge curves in cycle test for CPM based Li-S cell performed at 0.2 C. c) Rate capabilities of battery using different separators under the rate of 0.1, 0.2, 0.3, 0.5, 1, and 2 C. d) Long life cycle tests of Li-S cells with different separators at 0.2 C. e) Long life cycle tests of Li-S cells with CPM and PP separator at 1 C.

performed at 0.2 C for the 2nd cycle also indicated the function of CPM in reducing polarization (Figure S11, Supporting Information). The Li$^+$ transfer number (t_{Li+}) of the separator was also measured by Li//Li symmetric cell at room temperature. The t_{Li+} of the CPM was 0.80, which was higher than that of Ni$_3$(HITP)$_2$/PP (0.69) and COF/PP (0.60), yet almost similar to that of COF-IL/PP (0.81) (Figure 2e). The experimental results are consistent with our hypothesis that the CPM separator will provide a large available Li$^+$ flux and promote Li$^+$/electrolyte diffusion.

Based on this method mentioned above, the fabrication conditions of both sides in CPM can be easily tuned, including the thickness or loading of COF-IL layer and growth time (1, 3, 5, 10, 20 h) of Ni$_3$(HITP)$_2$ layer, thus producing a series of CPM separators to investigate their battery performances. Initially, the cycling performances of CPM separators with different COF-IL layer casting thicknesses (50–750 µm) had been evaluated by a constant current charge/discharge test at 0.2 C. For the casting thickness of about 50, 100, 250, and 750 µm, the initial

capacities of the corresponding Li-S cells were 1167.4, 1045.1, 1266.8, and 1517.7 mAh g^{-1}, and after 100 cycles, their capacities decreased to 264.5, 282.4, 674.6, and 233.7 mAh g^{-1}, respectively (Figure S12, Supporting Information). This indicates that 250 µm is the optimal thickness. Based on the optimized thickness, the cycling performances of the CPM separators with different COF-IL loadings (10–30 wt%) were investigated at 0.2 C. For 10, 15, 20, and 30 wt% loadings, the initial capacities of the corresponding Li-S cells were 847.8, 786.4, 1266.8, and 963.4 mAh g^{-1}, respectively. After 100 cycles, their capacities decreased to 361.4, and 266.1, 674.6, 374.1 mAh g^{-1}, indicating 20 wt% loading of COF-IL is the best one (Figure S13, Supporting Information). In addition, CPM separators with different Ni$_3$(HITP)$_2$ growth time (i.e., 1, 3, 5, 10, and 20 h) had also been explored. The initial capacities of CPM were 846.4, 1266.8, 1175.9, 1085.3, and 1246.6 mAh g^{-1} for the growth time of 1, 3, 5, 10, and 20 h, and decreased to 380.6 (after 20 cycles), 674.6, 162.1, 210.3, and 300.3 mAh g^{-1} after 100 cycles, respectively, suggesting 3 h to be the optimal time (Figure S14,

**ADVANCED
SCIENCE NEWS**

www.advancedsciencenews.com

NANO · MICRO

small

www.small-journal.com

Supporting Information). The performance may be related to the amount of $Ni_3(HITP)_2$ grown on PP surface at different time (Figures S15 and S16, Supporting Information).

The FT-IR spectrum of $Ni_3(HITP)_2$ layer of CPM after the test showed peaks at 1274 and 1054 cm^{-1} due to the generation of $Ni_3(HITP)_2$ with LiPSs,[48] further demonstrating the adsorption effect of S on Ni sites in CPM (Figure S17, Supporting Information). It was further confirmed by the SEM test that the morphology of the top and cross-sectional images after cell tests remained almost unchanged when compared to the initial state, implying the high durability of CPM during the cell test (Figure S18, Supporting Information). In addition, X-ray photoelectron spectroscopy (XPS) was also accomplished to check the composition of the CPM separator before and after cycling (Figures S19–S22, Supporting Information). S 2s and S 2p peaks can be obviously observed from both sides of CPM separator after cycling, which is derived from the interaction of MOF/COF-IL with LiPSs. For the COF-IL layer, in the deconvoluted S 2p XPS spectrum, the peaks at 164.0 and 163.0 eV were assigned to the bridging sulfur (S_B^0) and terminal sulfur (S_T^{-1}), respectively. Specifically, the peak of the S_T^{-1} bond at 162.6 eV was upshifted by 0.4 eV when compared to the S_T^{-1}—Li bond,[30] and thiosulfate (168.5 eV) and polythionate (169.6 eV) were detected, which could be ascribed to the interaction of COF-IL with LiPSs (Figure S19, Supporting Information). For the MOF layer, due to the formation of Ni—S bonds, Ni 2p peaks at 873.3 eV ($2p_{3/2}$) and 855.3 eV ($2p_{1/2}$) were changed to binding energies at 872.6 and 855.9 eV (Figure S21, Supporting Information). Similarly, the characteristic peaks at 169.4 and 170.5 eV also demonstrated that thiosulfate and polythionate were formed in the $Ni_3(HITP)_2$ layer, further proving the strong interaction between MOF and LiPSs (Figure S21, Supporting Information).[30,35,49]

2.3. Investigating Structure–Functional Relationships

In order to reveal the vital roles of different components in the anisotropically hybridized CPM separator and gain an atomic understanding of the charge/discharge process, we have further performed the DFT calculations. The associated free energy diagram (FEDs) and associated largest Gibbs energy among the elementary steps (ΔG^0_{max}) of discharge (positive direction) and charge (negative direction) processes were calculated and plotted in **Figure** 4a,b. For the anodic side, COF-IL layer has two possible reaction centers, namely, the IL group (i.e., 2-bromoethyltrimethylammonium bromide) and TPP (i.e., porphyrin N_4 sites). For the cathodic side, the active center of $Ni_3(HITP)_2$ layer is around the Ni–N_4 site. Optimized adsorption configurations of the three possible reaction centers are shown in Figure 4c, during which we choose the sites that bind most strongly to the adsorbate as the reaction sites for these three possible groups. For $Ni_3(HITP)_2$, the rate-limiting step is the transition from S_8 to Li_2S_8 with a ΔG of 0.91 eV, lower than the ΔG (1.27 eV) of the rate-limiting step for normal LiPSs conversion,[50] proving that $Ni_3(HITP)_2$ is beneficial for promoting LiPSs catalysis by lowering the energy barrier. This is consistent with our expected experimental results.

In addition, the binding energy of LiPSs and substrate has also been calculated to evaluate the adsorption capability (Figure 4d). The more positive or larger the binding energy value, the stronger the anchoring effect of Li_2S_x on the substrate is indicated. For $Ni_3(HITP)_2$, the binding energies for Li_2S_2, Li_2S_4, Li_2S_6, and Li_2S_8 were −1.22, −0.81, −0.90, −1.08 eV, respectively, indicating that $Ni_3(HITP)_2$ have strong chemical binding ability to LiPSs.[51] For COF-IL layer, a similar adsorption trend has been detected for TPP. Interestingly, the adsorption becomes much stronger for IL group and this trend can be seen more clearly in the collective of adsorption energies in Figure 4d. As COF-IL connects IL group with TPP, those two different adsorption styles generate an additional joint path (Figure S23, Supporting Information). That is, the Li_2S_8 and Li_2S_6 are made in TPP, while shifting to IL group to complete the leaving steps. As a consequence, we find that COF-IL gives high activity in both the discharge and charge process (Figure S24, Supporting Information), as indicated in the ΔG^0_{max} among the elementary steps plotted in Figure 4b. Hence, the good activity for both discharging and charging processes can be attributed to the cooperation of a high-reactive group (IL group) and a low-reactive group (TPP), which overcomes the originally strong adsorption of Li_2S_8 and Li_2S_6 for IL group, and the weak adsorptions of Li_2S and Li_2S_2 for TPP. Besides, we have also obtained the HOMO-LUMO energy levels of the IL group by DFT calculations (Figure 4e). The high Li$^+$ conductivity and low polarization are attributed to the relatively high HOMO energy level and low LUMO energy level of the IL group forming a lower energy barrier (E_{gap} = 2.68 eV) than that of LiTFSI (E_{gap} = 5.35 eV[52]), indicating it is more possible for IL group to participate in the reactions that take place at the interface with the Li anode, thereby contributing to the formation of a solid SEI layer (Figure 4e).[53–55] This is consistent with the above experimental results of the high t_{Li+} for both COF-IL/PP (0.81) and CPM (0.80) based symmetric cells, indicating the effect of COF-IL layer on Li$^+$/electrolyte transfer that can inhibit the formation of Li dendrites and effectively protect the anodic electrode. Combined with the efficient LiPSs adsorption/catalysis of $Ni_3(HITP)_2$ as mentioned above, such a kind of anisotropically hybridized CPM separator can directionally meet the multi-function requirements of both electrodes to achieve excellent battery performance.

3. Conclusion

In summary, we reported an anisotropically hybridized separator (CPM) based on an ionic liquid-modified porphyrin-based covalent-organic framework (COF-366-OH-IL) and catalytically active metal-organic framework ($Ni_3(HITP)_2$) that can integrate the LiPSs adsorption/catalytic conversion and ion-conduction sites together to directionally fulfill the requirements of electrodes. Both sides of the obtained hybrid separator exhibit uniform pore size distribution, favorable electrolyte wettability, robustness, and functional anisotropy. Notably, the-obtained separator exhibits an exceptional high Li$^+$ transference-number (t_{Li+} = 0.8), ultralow polarization-voltage (<30 mV), high initial specific-capacity (921.38 mAh g^{-1} at 1 C) and stable cycling-performance, much superior to PP and monolayer modified separators. Interestingly, DFT calculations also confirm the anisotropic effect of CPM on the anodic side (e.g., Li$^+$ transfer,
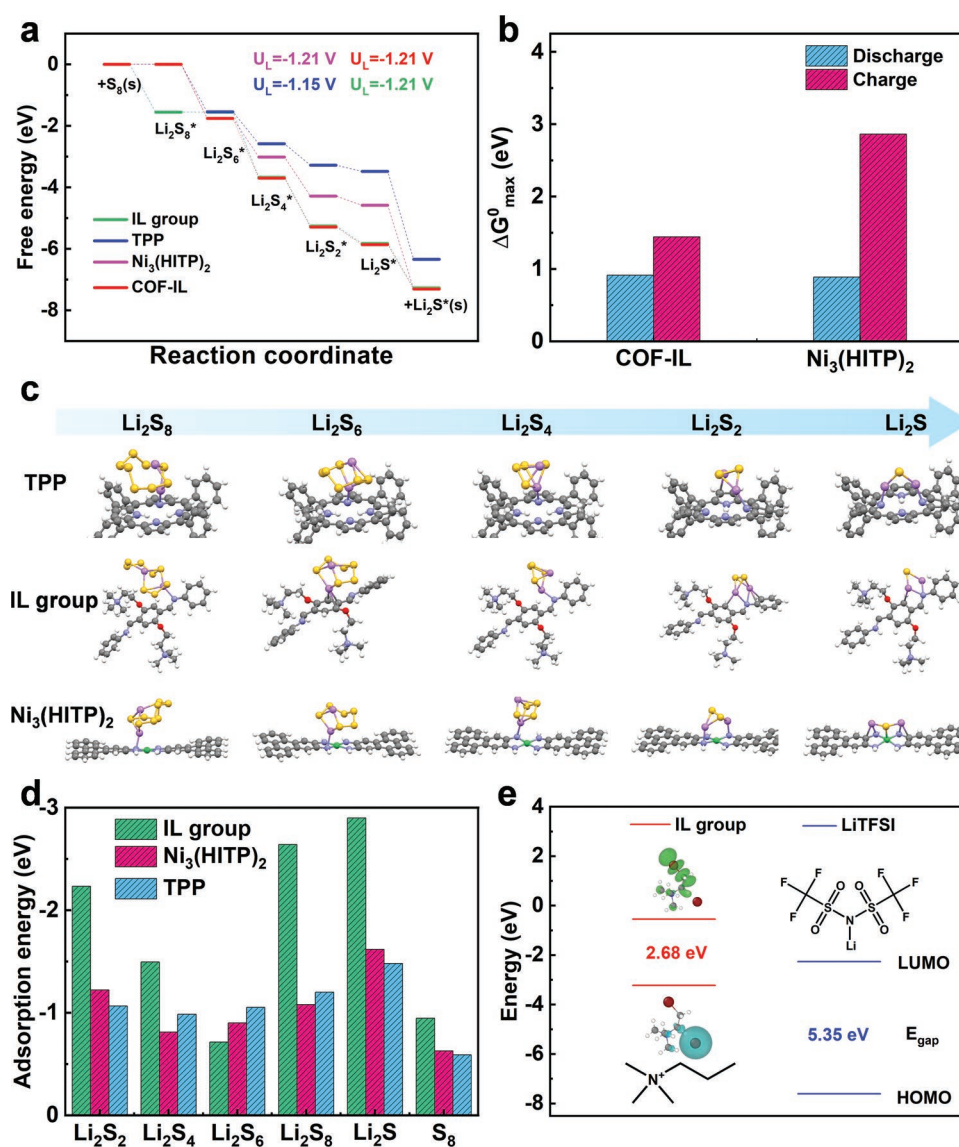
Figure 4. The DFT calculations of CPM based Li-S cells. a) The free energy diagram for the reduction of LiPSs on CPM. b) The largest Gibbs energy among the elementary steps of COF-IL and $Ni_3(HITP)_2$ in CPM. c) Optimized adsorption configurations of the reaction centers (above, TPP center; middle, IL group center and bottom, $Ni_3(HITP)_2$ center). d) The adsorption energies of Li_2S_x on different reaction centers in CPM. e) The HOMO-LUMO energy levels of the IL group and LiTFSI.

LiPSs adsorption and anode-protection) and cathodic side (e.g., LiPSs adsorption/catalysis). This work might provide new ideas or prospects for exploring functional anisotropically hybridized porous crystalline Li-S battery separators to meet the potential demand of next-generation battery system.

4. Experimental Section

Synthesis of COF-366-OH: The synthesis steps of COF-366-OH were based on the previously reported literatures.[39] A 10 mL schlenk tube was charged with TAPP (27 mg, 0.04 mм), DHA (13.3 mg, 0.08 mmol), ethanol (1 mL), 1, 2-dichlorobenzene (1 mL), and acetic acid (6 м, 0.2 mL). After sonication for about 20 min, the tube was flash-frozen at 77 K followed by three freeze-pump-thaw cycles and sealed. After the temperature returned to room temperature, it was then heated at 120 °C

for 72 h. A brown dark precipitate was isolated by filtration in Buchner funnel, followed by washing with THF. After that, the wet sample was transferred into a Soxhlet extractor and washed with THF (24 h). Finally, the product was evacuated at 100 °C under vacuum overnight to yield the activated sample.

Synthesis of COF-366-OH-IL: The synthesis steps of COF-366-OH-IL were based on the previously reported literatures.[40] K_2CO_3 (20 mg, 0.14 mmol), (2-bromoethyl)trimethylammonium bromide (101 mg, 0.41 mmol) and COF-366-OH (115 mg) were dispersed in THF (20 mL). Then, the mixture was heated at 65 °C and stirred for 24 h. The product was filtered, washed with THF, and then dried at 100 °C under vacuum for 12 h.

Synthesis of CPM Membranes: Taking CPM (20 wt%) for example, The COF-366-OH-IL with a mass fraction of 20 wt% was added into the PVDF-HFP solution in DMF of 0.2 g mL^{-1}, ball milled for 2 h and scraped onto the PP separator with a doctor blade (250 μm) and dry at 60 °C. Then, the other side of the separator was placed on the solution

surface of the mixed aqueous solution of $NiCl_2·6H_2O$ (2 mg mL^{-1}) and HITP (3 mg mL^{-1}) with 300 μL ammonia. After heating at 65 °C in an oven for 3 h, the obtained membrane was washed with ultrapure water and ethanol, and dried at 60 °C under vacuum.

Supporting Information

Supporting Information is available from the Wiley Online Library or from the author.

Conflict of Interest

The authors declare no conflict of interest.

Author Contributions

Y.Z. and C.G. contributed equally to this work. Y.-Q.L., Y.C., and Y.Z. conceived the idea. Y.Z. designed the experiments, collected, and analyzed the data. C.G.J.Z., X.Y., J.L., H.Z., and Y.C. assisted with the experiments and characterizations. Y.Z. wrote the manuscript. All authors have approved the final version of the manuscript.

Data Availability Statement

The data that support the findings of this study are available in the supplementary material of this article.

[1] A. Manthiram, Y. Fu, S. H. Chung, C. Zu, Y. S. Su, *Chem. Rev.* **2014**, *114*, 11751.

[2] G. M. Zhou, H. Chen, Y. Cui, *Nat. Energy* **2022**, *7*, 312.

[3] P. G. Bruce, S. A. Freunberger, L. J. Hardwick, J.-M. Tarascon, *Nat. Mater.* **2012**, *11*, 19.

[4] Y. Yang, G. Zheng, Y. Cui, *Chem. Soc. Rev.* **2013**, *42*, 3018.

[5] C.-X. Bi, M. Zhao, L.-P. Hou, Z.-X. Chen, X.-Q. Zhang, B.-Q. Li, H. Yuan, J.-Q. Huang, *Adv. Sci.* **2022**, *9*, 2103910.

[6] Y.-X. Yin, S. Xin, Y.-G. Guo, L.-J. Wan, *Angew. Chem., Int. Ed.* **2013**, *52*, 13186.

[7] A. Manthiram, Y. Fu, Y.-S. Su, *Acc. Chem. Res.* **2013**, *46*, 1125.

[8] R. Fang, S. Zhao, Z. Sun, W. Wang, H.-M. Cheng, F. Li, *Adv. Mater.* **2017**, *29*, 1606823.

[9] Z.-X. Chen, M. Zhao, L.-P. Hou, X.-Q. Zhang, B.-Q. Li, J.-Q. Huang, *Adv. Mater.* **2022**, *34*, 2201555.

[10] Z. Wei, Y. Ren, J. Sokolowski, X. Zhu, G. Wu, *InfoMat* **2020**, *2*, 483.

[11] N. Deng, W. Kang, Y. Liu, J. Ju, D. Wu, L. Li, B. S. Hassan, B. Cheng, *J. Power Sources* **2016**, *331*, 132.

[12] W. Kang, N. Deng, J. Ju, Q. Li, D. Wu, X. Ma, L. Li, M. Naebe, B. Cheng, *Nanoscale* **2016**, *8*, 16541.

[13] H.-J. Peng, J.-Q. Huang, X.-B. Cheng, Q. Zhang, *Adv. Energy Mater.* **2017**, *7*, 1700260.

[14] Z. A. Ghazi, X. He, A. M. Khattak, N. A. Khan, B. Liang, A. Iqbal, J. Wang, H. Sin, L. Li, Z. Tang, *Adv. Mater.* **2017**, *29*, 1606817.

[15] J. He, Y. Chen, A. Manthiram, *Energy Environ. Sci.* **2018**, *11*, 2560.

[16] G.-K. Gao, Y.-R. Wang, S.-B. Wang, R.-X. Yang, Y. Chen, Y. Zhang, C. Jiang, M.-J. Wei, H. Ma, Y.-Q. Lan, *Angew. Chem., Int. Ed.* **2021**, *60*, 10147.

[17] L. Fan, M. Li, X. Li, W. Xiao, Z. Chen, J. Lu, *Joule* **2019**, *3*, 361.

[18] H. Yao, K. Yan, W. Li, G. Zheng, D. Kong, Z. W. Seh, V. K. Narasimhan, Z. Liang, Y. Cui, *Energy Environ. Sci.* **2014**, *7*, 3381.

[19] Y. C. Jeong, J. H. Kim, S. Nam, C. R. Park, S. J. Yang, *Adv. Funct. Mater.* **2018**, *28*, 1707411.

[20] T. Tao, S. Lu, Y. Fan, W. Lei, S. Huang, Y. Chen, *Adv. Mater.* **2017**, *29*, 1700542.

[21] J.-F. Ding, R. Xu, R.-X. Ma, Y. Xiao, Y.-X. Yao, C. Yan, J.-Q. Huang, *Angew. Chem., Int. Ed.* **2022**, *61*, e202115602.

[22] W. Xia, A. Mahmood, R. Zou, Q. Xu, *Energy Environ. Sci.* **2015**, *8*, 1837.

[23] M. Du, Q. Li, Y. Zhao, C.-S. Liu, H. Pang, *Coord. Chem. Rev.* **2020**, *416*, 213341.

[24] M.-X. Wu, Y.-W. Yang, *Adv. Mater.* **2017**, *29*, 1606134.

[25] S. Mitra, H. S. Sasmal, T. Kundu, S. Kandambeth, K. Math, D. D. Diaz, R. Banerjee, *J. Am. Chem. Soc.* **2017**, *139*, 4513.

[26] S. Yuan, L. Feng, K. Wang, J. Pang, M. Bosch, C. Lollar, Y. Sun, J. Qin, X. Yang, P. Zhang, Q. Wang, L. Zou, Y. Zhang, L. Zhang, Y. Fang, J. Li, H.-C. Zhou, *Adv. Mater.* **2018**, *30*, 1704303.

[27] S. J. Datta, A. Mayoral, N. Murthy Srivatsa Bettahalli, P. M. Bhatt, M. Karunakaran, I. D. Carja, D. Fan, M. M. P. Graziane, R. Semino, G. Maurin, O. Terasaki, M. Eddaoudi, *Science* **2022**, *376*, 1080.

[28] Z. Hu, B. J. Deibert, J. Li, *Chem. Soc. Rev.* **2014**, *43*, 5815.

[29] X. Liu, D. Huang, C. Lai, G. Zeng, L. Qin, H. Wang, H. Yi, B. Li, S. Liu, M. Zhang, R. Deng, Y. Fu, L. Li, W. Xue, S. Chen, *Chem. Soc. Rev.* **2019**, *48*, 5266.

[30] Y. He, Z. Chang, S. Wu, Y. Qiao, S. Bai, K. Jiang, P. He, H. Zhou, *Adv. Energy Mater.* **2018**, *8*, 1802130.

[31] X.-J. Hong, C.-L. Song, Y. Yang, H.-C. Tan, G.-H. Li, Y.-P. Cai, H. Wang, *ACS Nano* **2019**, *13*, 1923.

[32] G.-K. Gao, Y.-R. Wang, H.-J. Zhu, Y. Chen, R.-X. Yang, C. Jiang, H. Ma, Y.-Q. Lan, *Adv. Sci.* **2020**, *7*, 2002190.

[33] J. Xu, S. An, X. Song, Y. Cao, N. Wang, X. Qiu, Y. Zhang, J. Chen, X. Duan, J. Huang, W. Li, Y. Wang, *Adv. Mater.* **2021**, *33*, 2105178.

[34] K. Sun, C. Wang, Y. Dong, P. Guo, P. Cheng, Y. Fu, D. Liu, D. He, S. Das, Y. Negishi, *ACS Appl. Mater. Interfaces* **2022**, *14*, 4079.

[35] D. Cai, M. Lu, L. Li, J. Cao, D. Chen, H. Tu, J. Li, W. Han, *Small* **2019**, *15*, 1902605.

[36] J. Zheng, J. Tian, D. Wu, M. Gu, W. Xu, C. Wang, F. Gao, M. H. Engelhard, J.-G. Zhang, J. Liu, J. Xiao, *Nano Lett.* **2014**, *14*, 2345.

[37] X. Hu, X. Jian, Z. Fang, L. Zhong, Z. Yuan, M. Yang, S. Ren, Q. Zhang, X. Chen, D. Yu, *Energy Storage Mater.* **2019**, *22*, 40.

[38] C. Guo, M. Liu, G.-K. Gao, X. Tian, J. Zhou, L.-Z. Dong, Q. Li, Y. Chen, S.-L. Li, Y.-Q. Lan, *Angew. Chem., Int. Ed.* **2022**, *61*, e202113315.

[39] S. Kandambeth, D. B. Shinde, M. K. Panda, B. Lukose, T. Heine, R. Banerjee, *Angew. Chem., Int. Ed.* **2013**, *52*, 13052.

[40] J. Qiu, Y. Zhao, Z. Li, H. Wang, Y. Shi, J. Wang, *ChemSusChem* **2019**, *12*, 2421.

[41] D. Sheberla, L. Sun, M. A. Blood-Forsythe, S. Er, C. R. Wade, C. K. Brozek, A. Aspuru-Guzik, M. Dinca, *J. Am. Chem. Soc.* **2014**, *136*, 8859.

[42] Y. Zang, F. Pei, J. Huang, Z. Fu, G. Xu, X. Fang, *Adv. Energy Mater.* **2018**, *8*, 1802052.

[43] X. Chen, M. Addicoat, E. Jin, L. Zhai, H. Xu, N. Huang, Z. Guo, L. Liu, S. Irle, D. Jiang, *J. Am. Chem. Soc.* **2015**, *137*, 3241.

[44] M. Li, Y. Wan, J.-K. Huang, A. H. Assen, C.-E. Hsiung, H. Jiang, Y. Han, M. Eddaoudi, Z. Lai, J. Ming, L.-J. Li, *ACS Energy Lett.* **2017**, *2*, 2362.

[45] G. Zhang, Z.-W. Zhang, H.-J. Peng, J.-Q. Huang, Q. Zhang, *Small Methods* **2017**, *1*, 1700134.

[46] R. Xu, J. Lu, K. Amine, *Adv. Energy Mater.* **2015**, *5*, 1500408.

[47] Y. Li, W. Wang, X. Liu, E. Mao, M. Wang, G. Li, L. Fu, Z. Li, A. Y. S. Eng, Z. W. Seh, Y. Sun, *Energy Storage Mater.* **2019**, *23*, 261.

[48] H. Chen, Y. Xiao, C. Chen, J. Yang, C. Gao, Y. Chen, J. Wu, Y. Shen, W. Zhang, S. Li, F. Huo, B. Zheng, *ACS Appl. Mater. Interfaces* **2019**, *11*, 11459.

[49] L. Zhang, D. Liu, Z. Muhammad, F. Wan, W. Xie, Y. Wang, L. Song, Z. Niu, J. Chen, *Adv. Mater.* **2019**, *31*, 1903955.

[50] J. Wang, F. Li, Z. Liu, Z. Dai, S. Gao, M. Zhao, *ACS Appl. Mater. Interfaces* **2021**, *13*, 61205.

[51] G. Li, X. Wang, M. H. Seo, M. Li, L. Ma, Y. Yuan, T. Wu, A. Yu, S. Wang, J. Lu, Z. Chen, *Nat. Commun.* **2018**, *9*, 705.

[52] Y. He, Y. Zhang, P. Yu, F. Ding, X. Li, Z. Wang, Z. Lv, X. Wang, Z. Liu, X. Huang, *J. Energy Chem.* **2020**, *45*, 1.

[53] Q. Zhou, J. Ma, S. Dong, X. Li, G. Cui, *Adv. Mater.* **2019**, *31*, 1902029.

[54] K. Liu, Z. Wang, L. Shi, S. Jungsuttiwong, S. Yuan, *J. Energy Chem.* **2021**, *59*, 320.

[55] D. Wang, H. Liu, M. Li, D. Xia, J. Holoubek, Z. Deng, M. Yu, J. Tian, Z. Shan, S. P. Ong, P. Liu, Z. Chen, *Nano Energy* **2020**, *75*, 104889.